Drug Screening Hot Paper

Deutsche Ausgabe: DOI: 10.1002/ange.201503141
Internationale Ausgabe: DOI: 10.1002/anie.201503141

Pim Kinase Inhibitors Evaluated with a Single-Molecule Engineered Nanopore Sensor**

*Leon Harrington, Leila T. Alexander, Stefan Knapp, and Hagan Bayley**

Abstract: *Protein kinases are critical therapeutic targets. Pim kinases are implicated in several leukaemias and cancers. Here, we exploit a protein nanopore sensor for Pim kinases that bears a pseudosubstrate peptide attached by an enhanced engineering approach. Analyte binding to the sensor peptide is measured through observation of the modulation of ionic current through a single nanopore. We observed synergistic binding of MgATP and kinase to the sensor, which was used to develop a superior method to evaluate Pim kinase inhibitors featuring label-free determination of inhibition constants. The procedure circumvents many sources of bias or false-positives inherent in current assays. For example, we identified a potent inhibitor missed by differential scanning fluorimetry. The approach is also amenable to implementation on high throughput chips.*

There are over five hundred kinases encoded in the human genome,[1] which regulate most cellular processes by the transfer of phosphate from ATP to protein substrates. Protein kinases are overexpressed or dysregulated in many diseases. Spurred on by high-profile successes such as imatinib (Gleevec),[2] protein kinases are under intense investigation as therapeutic targets in drug discovery programs. The Pim kinases are a family of three serine/threonine kinases that regulate several downstream processes essential for cancer progression, and whose overexpression has been implicated in a number of cancers and leukemias.[3] Here, we describe the development of a single-molecule, nanopore-based assay for the evaluation of Pim kinase inhibitors that exploits a detection method that differs radically from prevailing methods.

While radiometric assays are widely regarded as the gold standard for protein kinases, homogeneous "mix and measure" assays utilizing fluorescence detection predominate, as they are easy to automate and do not require radioisotopes.[4] Nonetheless, these assays may still require costly reagents such as labeled antibodies, and are often susceptible to interference from colored or fluorescent compounds, or inhibition of coupled enzyme reactions. Differential scanning fluorimetry (DSF) measures the stabilization of a protein fold to thermal denaturation contributed by ligand binding, and has found favor due to its cost-effectiveness and scalability.[5] This is at the expense of accuracy, as DSF measurements are less directly correlated to ligand affinity than direct determinations of inhibition constants or half-maximal inhibitory concentrations (IC50 values).[6]

We have previously developed a novel engineering strategy for producing heptameric alpha-hemolysin (αHL) pores containing a single subunit bearing a peptide sensor element fused to the *trans* mouth loop.[7] Site-specific proteolysis liberates one end of the sensor-element so that it is attached by a single peptide bond (Figure 1a). Analyte binding is readily observed by monitoring the modulation of ionic current flow through a single pore in an artificial membrane under an applied potential.

In the present work, we applied this strategy to engineer a pseudosubstrate analogue of the Pim consensus substrate sequence "Pimtide" as the sensor element (Figure 1a,b).[7,8] This allowed us to measure kinase binding to the sensor in the presence of MgATP without subsequent phosphorylation. We discovered synergistic binding to Pim-1 by MgATP and the sensor peptide. Inhibition constants of ATP-competitive inhibitors could be determined by measuring their modulation of the synergistic binding. Evaluation of a small test set of compounds identified a potent inhibitor missed by DSF, suggesting that our approach is more robust. This establishes a novel, label-free inhibitor-screening procedure amenable to scaling to high-throughput when coupled with parallel measurement technologies. Further, the determination of hitherto unknown parameters, such as the affinity of MgATP for Pim-1, provides new insight into the Pim kinase mechanism and demonstrates the power and versatility of our technique.

The new heteroheptameric, pseudo-substrate-functionalized pore, $(\alpha HL\text{-}D127N\text{-}PSLM\text{-}TEV\text{-}D8)_1(\alpha HL\text{-}D127N)_6$ (hereafter αHL-D127N-PSLM-TEV), exhibited similar two-state gating behavior to the previously described αHL-

[*] Dr. L. Harrington,[+] Prof. Dr. H. Bayley
Department of Chemistry, University of Oxford
12 Mansfield Road, Oxford, OX1 3TA (UK)
E-mail: hagan.bayley@chem.ox.ac.uk
Dr. L. T. Alexander,[++] Prof. Dr. S. Knapp
Nuffield Department of Clinical Medicine, Structural Genomics Consortium and Target Discovery Institute, University of Oxford
Oxford, OX3 7DQ (UK)
[+] Present address: Max-Planck-Institut für Biochemie
Am Klopferspitz 18, 82152 Martinsried (Germany)
[++] Present address: Institute of Molecular Systems Biology, ETH Zurich, 8093 Zurich (Switzerland)

[**] We thank Clara Redondo for assistance with differential scanning fluorimetry. This work was supported by grants from the National Institutes of Health and Oxford Nanopore Technologies. L.H. was supported in part by a Biotechnology and Biological Sciences Research Council doctoral training grant. S.K. and L.T.A. are supported by the Structural Genomics Consortium, a registered charity (number 1097737) that receives funds from AbbVie, Boehringer Ingelheim, the Canada Foundation for Innovation, the Canadian Institutes for Health Research, Genome Canada, GlaxoSmithKline, Janssen, Lilly Canada, the Novartis Research Foundation, the Ontario Ministry of Economic Development and Innovation, Pfizer, Takeda, and the Wellcome Trust [092809/Z/10/Z].

Supporting information for this article is available on the WWW under http://dx.doi.org/10.1002/anie.201503141.

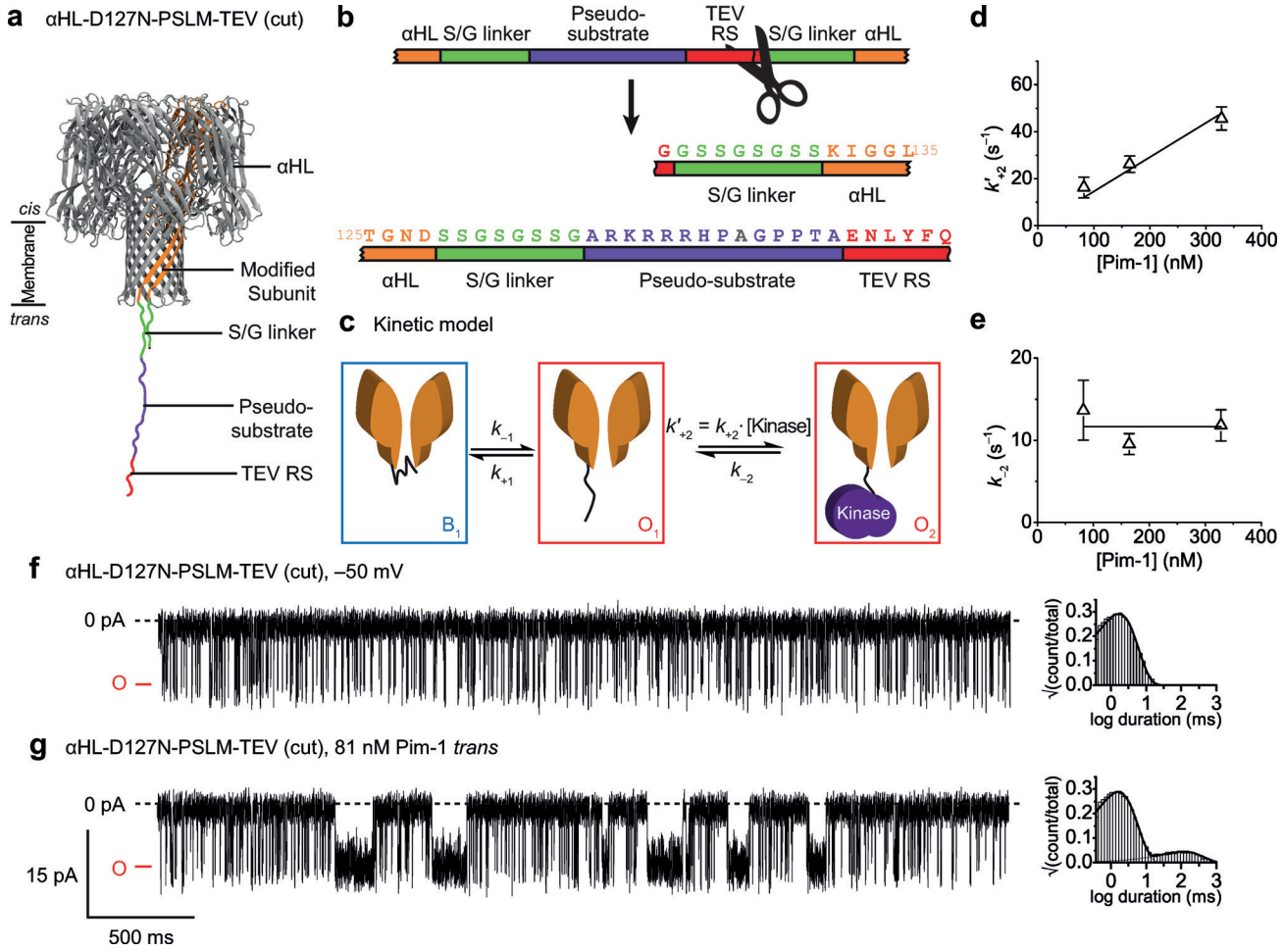

Figure 1. Sensor design and characterization. a) Illustration of the protease-cleaved sensor αHL-D127N-PSLM-TEV indicating the location of the pseudosubstrate sensor element (purple) flanked by serine/glycine linkers (green) and a TEV protease recognition site ("TEV RS", red). b) Design of the TEV protease-cleavable *trans* loop fusion within αHL-D127N-PSLM-TEV. c) Kinetic model for the analysis of the observed current signal through the αHL-D127N-PSLM-TEV (cut) sensor in the presence of Pim-1. State B_1 corresponds to the blocked current level of the pore due to occlusion by the attached peptide. State O_1 corresponds to the open pore that is not bound to a kinase, and O_2 corresponds to the open pore with a kinase molecule bound to the sensor peptide. Plots are shown of the concentration-dependence of d) the pseudo-first-order Pim-1 association rate constant k'_{+2} and e) the first-order Pim-1 dissociation rate constant k_{-2}. Error bars represent standard deviation (s.d.) ($n=4$). Representative current traces of the αHL-D127N-PSLM-TEV (cut) pore under an applied potential of −50 mV before (f) and after (g) the addition of 81 nM Pim-1 to the *trans* chamber are shown together with representative dwell-time histograms for the open-pore current level. The open-pore current level is marked "O". Measurements were performed in 15 mM MOPS, pH 6.8, 300 mM KCl, 5 mM DTT. The filter corner frequency was 2 kHz.

D127N-PLM-TEV[7] when inserted into planar lipid bilayers (Figure 1c–g).

In the absence of kinase, the mean blockade duration was 11 ± 3 ms, and the mean inter-event interval was 1.7 ± 0.3 ms (both $n=4$). With the same kinetic model as used for αHL-D127N-PLM-TEV (Figure 1c), we characterized the binding of Pim-1 to αHL-D127N-PSLM-TEV. The bimolecular association rate constant, dissociation rate constant, and dissociation equilibrium constant were: $k_{+2}=(1.5\pm0.1)\times10^8\,\text{M}^{-1}\,\text{s}^{-1}$, $k_{-2}=12\pm1\,\text{s}^{-1}$, $K_d=80\pm10$ nM (all $n=4$); the same as for αHL-D127N-PLM-TEV, within error (Figure 1d,e).

We next measured the effect of Mg^{2+} on the Pim-1-pseudosubstrate interaction. Mg^{2+} is required for ATP binding to kinases, but may also affect the kinase-pseudosubstrate interaction by both increasing the ionic strength of the solution and specifically binding within the active site.[9] We measured Pim-1 binding to the sensor before and after the addition of 10 mM $MgCl_2$ (final concentration). Upon addition of $MgCl_2$, k_{+2} decreased from $(1.3\pm0.2)\times10^8\,\text{M}^{-1}\text{s}^{-1}$ to $(8.7\pm0.2)\times10^7\,\text{M}^{-1}\text{s}^{-1}$, and k_{-2} increased from $12\pm3\,\text{s}^{-1}$ to $18\pm4\,\text{s}^{-1}$ (all $n=12$). K_d increased from 90 ± 20 nM to 210 ± 60 nM ($n=12$).

Addition of ATP in the presence of 10 mM $MgCl_2$ gave rise to a new population of events in the open-pore current level with a mean duration of several seconds, additional to shorter duration populations corresponding to apo-Pim-1 binding and pore blockade by the sensor peptide (Figure 2a). We hypothesized that the additional population corresponds to the ternary complex between Pim-1, MgATP, and the sensor peptide, consistent with synergistic binding.

Assuming independent binding of apo-Pim-1 and Pim-1-MgATP to the sensor, we modified our kinetic model and

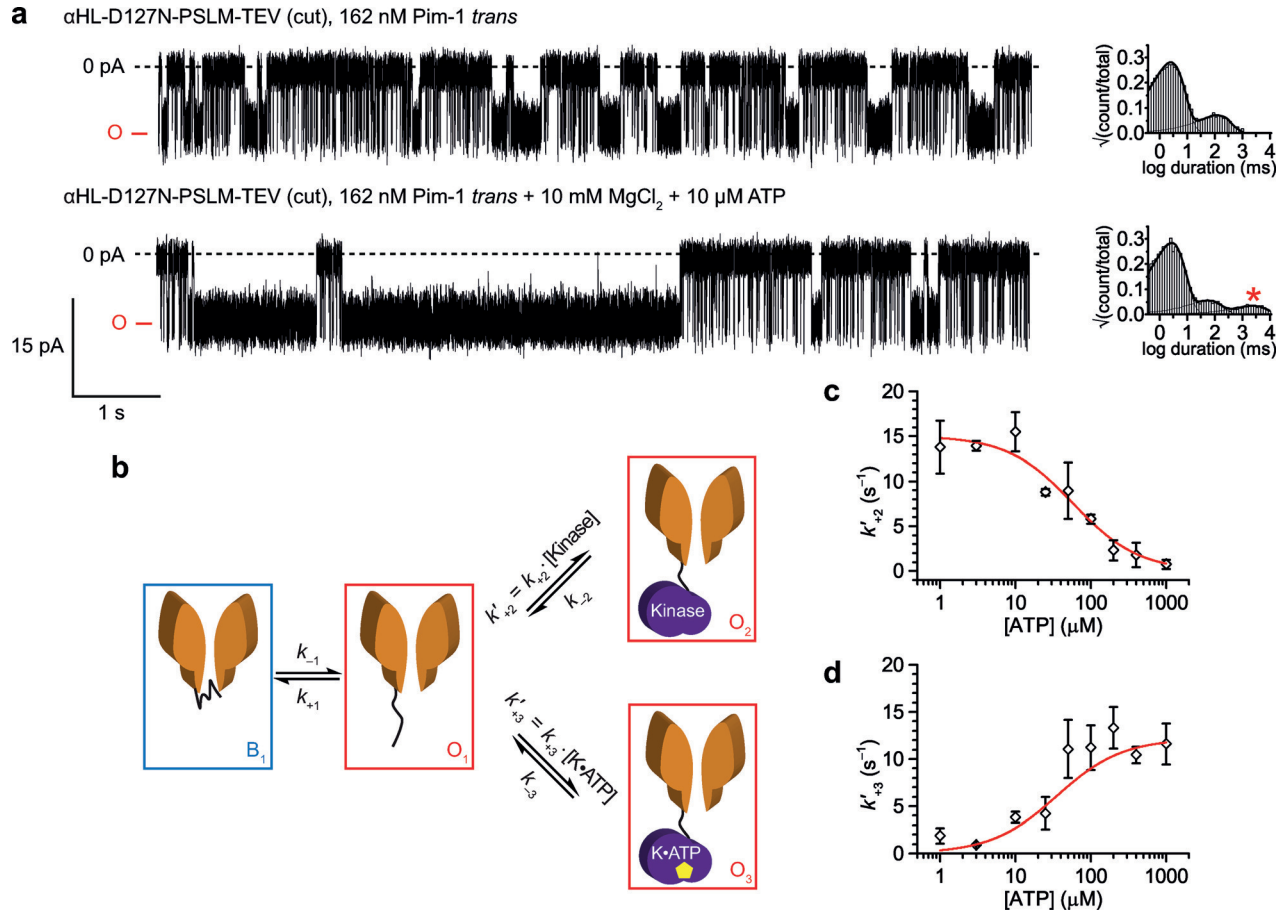

Figure 2. Effect of MgATP on Pim-1 interaction with sensor. a) Representative current traces and open-pore current level dwell-time histograms of αHL-D127N-PSLM-TEV (cut) under an applied potential of −50 mV in the presence of 162 nM Pim-1 before and after the addition of 10 mM $MgCl_2$ and 10 μM ATP to the *trans* chamber. The open-pore current level is marked "O". The additional population of events corresponding to ternary complex formation is marked with a red asterisk. b) Kinetic model for the current signal observed in the presence of Pim-1 and MgATP. States are as in Figure 1c, with the addition of O_3, which corresponds to the open pore where kinase-MgATP binds to the sensor peptide to form a ternary complex. Note: an additional blocked state B_2 connected to O_3 (not shown) was included to properly account for "noise" spikes[7] during long events corresponding to the ternary complex (SI). The ATP concentration-dependence of the pseudo-first-order association rate constants for formation of the c) binary (k'_{+2}) and d) ternary (k'_{+3}) complex are plotted together with their fitted curves according to Equations (1) and (2), respectively. The concentration of Pim-1 was 162 nM throughout. Error bars represent s.d. ($n=3$). Measurements were performed in 15 mM MOPS, pH 6.8, 300 mM KCl, 5 mM DTT. The filter corner frequency was 2 kHz.

derived equations relating the measured pseudo-first-order association rate constants for the binary (k'_{+2}) and ternary (k'_{+3}) complexes to the total concentration of ATP (Figure 2b, Supporting Information):

$$\frac{k'_{+2}}{[\mathrm{Pim}]_0} = k_{+2}\left(1 - \frac{[\mathrm{ATP}]_0}{K_d^{\mathrm{Pim\cdot MgATP}} + [\mathrm{ATP}]_0}\right) \quad (1)$$

$$\frac{k'_{+3}}{[\mathrm{Pim}]_0} = k_{+3}\left(\frac{[\mathrm{ATP}]_0}{K_d^{\mathrm{Pim\cdot MgATP}} + [\mathrm{ATP}]_0}\right) \quad (2)$$

Titration of ATP over a range of 1–1000 μM in the presence of 10 mM $MgCl_2$ confirmed that, in accordance with Equations (1) and (2), the frequency of events corresponding to ternary complex formation increased with ATP concentration, while the frequency of events corresponding to binary complex formation decreased (Figure 2c,d). Fitting of Equations (1) and (2) yielded $K_d^{\mathrm{Pim\cdot MgATP}}$ values of 60 ± 10 μM from the k'_{+2} data, and 35 ± 5 μM from the k'_{+3} data. The fitted value of k_{+2} was $(9.3\pm0.6)\times10^7\,\mathrm{M^{-1}s^{-1}}$, and k_{+3} was $(7.5\pm0.7)\times10^7\,\mathrm{M^{-1}s^{-1}}$.

The dissociation rate constant attributed to the binary complex, k_{-2}, shifted from $18\pm4\,\mathrm{s^{-1}}$ to $26\pm8\,\mathrm{s^{-1}}$ in the presence of ATP (mean calculated over 1–50 μM ATP, $n=15$; k_{-2} was fixed to the latter value when fitting dwell time histograms at higher ATP concentrations, where the binary population was sparse). We tested whether this shift might be due to ADP contamination. After the addition of ADP in the presence of 10 mM $MgCl_2$ and absence of ATP, we continued to see a single population of binding events (Supporting Information (SI), Figure S1a). While the association rate constant for this population was unaffected, the dissociation rate constant increased significantly with ADP concentration (SI, Figure S1b). Rarely, much longer events were seen, presumably due to contaminating ATP from ADP dispro-

portionation. Therefore, the shift in binary dissociation rate constant in the presence of ATP most likely results from contaminating ADP. As the association rate constant of the Pim-1-ADP complex is the same as that for apo-Pim-1, low levels of ADP should have a negligible effect on $K_d^{\text{Pim·MgATP}}$ determination from the "binary" event population (SI).

We also observed an ATP-dependent decrease in the dissociation rate constant for the ternary complex, k_{-3}, leveling off to a value of ca. $0.09\,s^{-1}$ at 1 μM ATP (SI, Figure S2). The origin of this effect is unclear, but may be due to the breakdown of some of our assumptions at low ATP concentrations, such as the assumption of independent binding of apo-Pim-1 and Pim-1-MgATP.

K_d values for MgATP with Pim-1 have not previously been reported. K_m values for MgATP with Pim-1 have been reported to be 10 μM[10] or 400 μM.[11] Our $K_d^{\text{Pim·MgATP}}$ values (60 and 35 μM, from binary and ternary populations respectively) appear reasonable when compared to other kinases; for example, the K_d of MgATP with cAMP-dependent protein kinase (PKA) was previously determined to be 25 μM.[12] This similarity of affinity is despite the Pim kinases lacking a highly conserved backbone NH hydrogen bond between a residue in the hinge region and ATP.[13] Synergistic binding between MgATP and an inhibitory peptide (PKIP5–24) to PKA has previously been observed.[12,14] Surface plasmon resonance (SPR) measurements found that this was largely due to k_{-3} being roughly four orders of magnitude lower than k_{-2}.[15] The effect for Pim-1 is similar, though smaller in magnitude. That k_{-3} is so much less than k_{-2}, and much slower than k_{cat} ($4\,s^{-1}$),[16] suggests that almost all productive complexes result in phosphorylation (see SI for further discussion). Together with rapid, electrostatically enhanced association rates,[7] these features ensure effective signal transduction even at very low kinase/substrate concentrations.

We reasoned that it should be possible to measure the modulation of synergistic binding by ATP-competitive inhibitors, and so determine inhibition constants (SI). We first had to confirm that Pim-1-inhibitor complexes would bind the sensor peptide, and compare the kinetics of this interaction with those for apo-Pim-1. We titrated the ATP-competitive Pim kinase inhibitor **1** (Figure 3a)[17] against the Pim-1-sensor interaction in the absence of ATP. Over the range 1–10000 nM of **1**, we observed a single population of binding events with similar kinetics as those seen when only Pim-1 was present (SI, Figure S3a,b). We could therefore treat events due to Pim-1-sensor binary complex formation and those due to the Pim-1-inhibitor-sensor complex as a single population, justifying the simplifying assumption that $k_{+2} \approx k_{+4}$ (where k_{+4} is the association rate constant of the Pim-1-inhibitor complex, SI). For simplicity, we continue to use the kinetic model in Figure 2b, and the notation k'_{+2}, where this now refers to the combined population of apo-Pim-1 and Pim-1-inhibitor binding events.

We next titrated **1** over the range 1–10000 nM against 100 μM ATP in the presence of 10 mM $MgCl_2$ and 162 nM Pim-1.

The frequency of ternary complex events decreased with increasing **1**, with a corresponding increase in frequency of the combined population of apo-Pim-1 and Pim-1-inhibitor

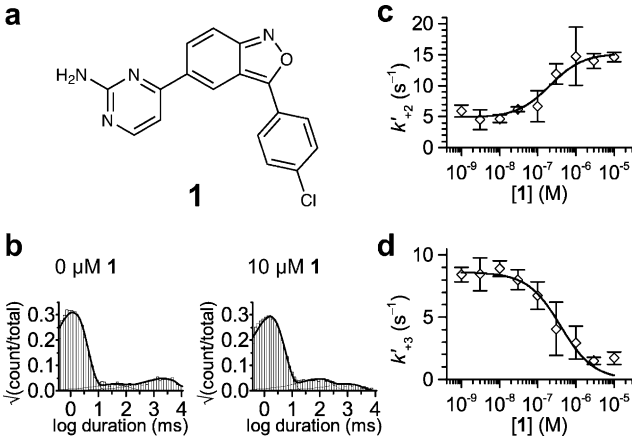

Figure 3. Determination of the inhibition constant for an ATP-competitive inhibitor of Pim-1. a) Chemical structure of compound **1**. b) Representative open-pore current level histograms before and after the addition of 10 μM **1** to the *trans* chamber, in the presence of 10 mM $MgCl_2$ and 100 μM ATP. The dependences of the pseudo-first-order association rate constants for formation of c) the combined Pim-1 and Pim-1-inhibitor "binary" population (where $k'_{+2} \approx k'_{+4}$, SI) and d) the ternary (k'_{+3}) complex on the concentration of **1** are plotted together with their fitted curves according to Equations (3) and (4), respectively. The concentration of Pim-1 was 162 nM throughout. Error bars represent s.d. ($n = 3$). Measurements were performed in 15 mM MOPS, pH 6.8, 300 mM KCl, 5 mM DTT. The filter corner frequency was 2 kHz.

binding events (Figure 3b). Plots of the dependence of the pseudo-first-order association rate constants k'_{+2} and k'_{+3} on the concentration of **1** were fitted with:

$$\frac{k'_{+2}}{[\text{Pim}]_0} = k_{+2}\frac{\left(1+\frac{[\text{I}]_0}{K_i}\right)}{\left(1+\frac{[\text{ATP}]_0}{K_d^{\text{Pim·MgATP}}}+\frac{[\text{I}]_0}{K_i}\right)} \quad (3)$$

and:

$$\frac{k'_{+3}}{[\text{Pim}]_0} = k_{+3}\frac{[\text{ATP}]_0}{K_d^{\text{Pim·MgATP}}\left(1+\frac{[\text{ATP}]_0}{K_d^{\text{Pim·MgATP}}}+\frac{[\text{I}]_0}{K_i}\right)} \quad (4)$$

respectively (SI). Values of the inhibition constant, K_i, were determined to be 70 ± 30 nM from the k'_{+2} curve, and 130 ± 30 nM from the k'_{+3} curve (Figure 3c,d). These compare well with a previously determined value (91 nM).[17] The bimolecular association rate constants for formation of the binary and ternary complexes were $k_{+2} = (9.4 \pm 0.5) \times 10^7\,M^{-1}s^{-1}$, and $k_{+3} = (7.8 \pm 0.3) \times 10^7\,M^{-1}s^{-1}$, respectively. During fitting, $K_d^{\text{Pim·MgATP}}$ was fixed to the mean of the two values determined above (47 μM).

Interestingly, ≥ 100 nM of **1** reversed the previously observed ATP-induced shift in k_{-2} when in the presence of MgATP and absence of inhibitor. We earlier ascribed the ATP-induced shift to traces of ADP, and so inhibitor-induced reversal of this shift must arise because the inhibitor outcompetes ADP.

To further validate our screening approach, we surveyed five additional compounds in a simple assay aimed at identifying those that bind below a defined affinity threshold. We first measured compounds **2–6** binding to Pim-1 by DSF

for reference. Compounds **2–3** appeared to bind Pim-1 strongly (IC50 ≈ 100 nM, based on previous correlations between temperature shift and IC50 values[6]), with **4–6** showing weak or no binding (IC50 ≥ 1 μM, Figure 4a). We then screened the compounds using our nanopore sensor at a concentration of 1 μM against 100 μM ATP in the presence of 10 mM $MgCl_2$ and 162 nM Pim-1. Compounds **2–4** appeared to bind with similar affinities as **1**, whereas **5** and **6** showed no effect, as determined from the pseudo-first-order association rate constants for the binary (combined apo-Pim-1 and Pim-1-inhibitor) and ternary (Pim-1-MgATP) events (Figure 4b,c).

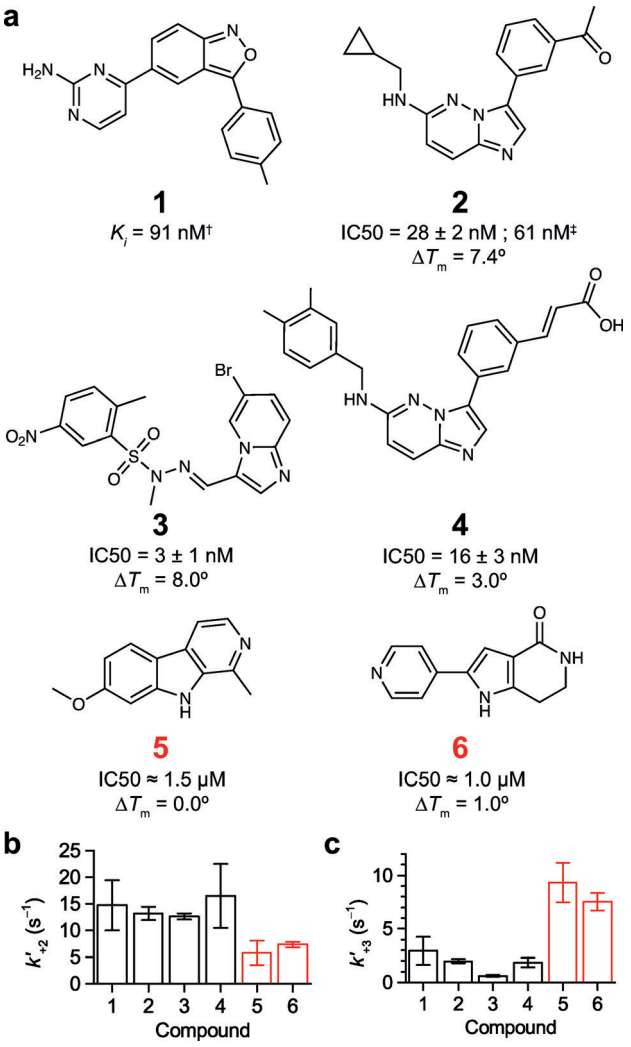

Figure 4. Screen of a panel of compounds against Pim-1. a) Structures of evaluated compounds are shown with thermal shift values determined by DSF and other relevant affinity/potency measurements. † Literature value for inhibition constant.[17] ‡ Literature value included for comparison.[18] All other IC50 values were determined in this work by a coupled-enzyme kinase assay.[18] Corresponding dose-response curves are shown in the SI, Figure S4. Values of the pseudo-first-order association rate constants in the presence of the compounds shown in (a) are plotted for b) the combined population of apo-Pim-1 and Pim-1-inhibitor binding events ("binary"' population, where $k'_{+2} \approx k'_{+4}$) and c) the ternary (k'_{+3}) complex ($n = 3$, in all cases). Compounds that bind at or above an affinity threshold of ca. 1 μM are highlighted by red numerals and bars. All compounds were used at a final concentration of 1 μM against 100 μM ATP. The concentration of Pim-1 was 162 nM. Measurements were performed in 15 mM MOPS, pH 6.8, 300 mM KCl, 5 mM DTT and 10 mM $MgCl_2$. The filter corner frequency was 2 kHz.

While DSF suggested that **4** should bind Pim-1 weakly, our nanopore screen suggested affinity similar to **1** and **2**, which the literature indicates are much more potent (K_i = 91 nM for **1**, IC50 = 61 nM for **2**). To seek clarification, we determined IC50 values for compounds **2–6** with a coupled-enzyme kinase assay (SI, Figure S4).[18] These IC50 values correlated well with our nanopore screen, indicating that DSF had not accurately determined the potency of **4**. Indeed, it has been previously noted that weaker hits identified by DSF are sometimes found to inhibit potently in enzymatic assays.[19] This finding exemplifies the benefits of K_i determination by our technique.

To be truly useful for high-throughput screening, many individual sensor pores will need to be monitored in parallel. Fortunately, this has been extensively pursued for the goal of nanopore DNA sequencing.[20,21] For example, Oxford Nanopore Technologies' MinION device is capable of monitoring hundreds of pores simultaneously (www.nanoporetech.com) and should be adaptable to inhibitor screening by incorporating microfluidic channels for compound delivery. Parallel measurement and bilayer miniaturization (for example droplet interface bilayers[22]) will ensure economical consumption of kinase. Further, consensus peptides for many kinases have been obtained from degenerate library arrays.[8] Through its markedly different basis of detection, our technique therefore offers a highly complementary means of inhibitor screening, yielding inhibition constants while avoiding biases inherent in existing methods, and with the prospect of scaling to high throughput.

Keywords: drug discovery · inhibitors · protein kinases · screening · single-molecule studies

How to cite: *Angew. Chem. Int. Ed.* **2015**, *54*, 8154–8159
Angew. Chem. **2015**, *127*, 8272–8277

[1] G. Manning, D. B. Whyte, R. Martinez, T. Hunter, S. Sudarsanam, *Science* **2002**, *298*, 1912–1934.
[2] R. Ohno, *Int. J. Clin. Oncol.* **2006**, *11*, 176–183.
[3] C. Blanco-Aparicio, A. Carnero, *Biochem. Pharmacol.* **2013**, *85*, 629–643.
[4] H. Ma, S. Deacon, K. Horiuchi, *Expert Opin. Drug Discovery* **2008**, *3*, 607–621.
[5] O. Fedorov, F. H. Niesen, S. Knapp, *Methods Mol. Biol.* **2012**, *795*, 109–118.
[6] O. Fedorov, B. Marsden, V. Pogacic, P. Rellos, S. Müller, A. N. Bullock, J. Schwaller, M. Sundström, S. Knapp, *Proc. Natl. Acad. Sci. USA* **2007**, *104*, 20523–20528.
[7] L. Harrington, S. Cheley, L. T. Alexander, S. Knapp, H. Bayley, *Proc. Natl. Acad. Sci. USA* **2013**, *110*, E4417–E4426.
[8] J. E. Hutti, E. T. Jarrell, J. D. Chang, D. W. Abbott, P. Storz, A. Toker, L. C. Cantley, B. E. Turk, *Nat. Methods* **2004**, *1*, 27–29.
[9] J. A. Adams, *Chem. Rev.* **2001**, *101*, 2271–2290.
[10] X. Wang, S. Magnuson, R. Pastor, E. Fan, H. Hu, V. Tsui, W. Deng, J. Murray, M. Steffek, H. Wallweber, J. Moffat, J. Drummond, G. Chan, E. Harstad, A. J. Ebens, *Bioorg. Med. Chem. Lett.* **2013**, *23*, 3149–3153.
[11] P. D. Garcia, J. L. Langowski, Y. Wang, M. Chen, J. Castillo, C. Fanton, M. Ison, T. Zavorotinskaya, Y. Dai, J. Lu, X. H. Niu, S. Basham, J. Chan, J. Yu, M. Doyle, P. Feucht, R. Warne, J.

Narberes, T. Tsang, C. Fritsch, A. Kauffmann, E. Pfister, P. Drueckes, J. Trappe, C. Wilson, W. Han, J. Lan, G. Nishiguchi, M. Lindvall, C. Bellamacina, J. A. Aycinena, R. Zang, J. Holash, M. T. Burger, *Clin. Cancer Res.* **2014**, *20*, 1834 – 1845.
[12] J. Lew, N. Coruh, I. Tsigelny, S. Garrod, S. S. Taylor, *J. Biol. Chem.* **1997**, *272*, 1507 – 1513.
[13] K. C. Qian, L. Wang, E. R. Hickey, J. Studts, K. Barringer, C. Peng, A. Kronkaitis, J. Li, A. White, S. Mische, B. Farmer, *J. Biol. Chem.* **2005**, *280*, 6130 – 6137.
[14] H. Xie, O. Braha, L.-Q. Gu, S. Cheley, H. Bayley, *Chem. Biol.* **2005**, *12*, 109 – 120.
[15] B. Zimmermann, J. A. Chiorini, Y. Ma, R. M. Kotin, F. W. Herberg, *J. Biol. Chem.* **1999**, *274*, 5370 – 5378.
[16] M. D. Jacobs, J. Black, O. Futer, L. Swenson, B. Hare, M. Fleming, K. Saxena, *J. Biol. Chem.* **2005**, *280*, 13728 – 13734.
[17] A. C. Pierce, M. Jacobs, C. Stuver-Moody, *J. Med. Chem.* **2008**, *51*, 1972 – 1975.
[18] A. N. Bullock, J. E. Debreczeni, O. Y. Fedorov, A. Nelson, B. D. Marsden, S. Knapp, *J. Med. Chem.* **2005**, *48*, 7604 – 7614.
[19] O. Fedorov, K. Huber, A. Eisenreich, P. Filippakopoulos, O. King, A. N. Bullock, D. Szklarczyk, L. J. Jensen, D. Fabbro, J. Trappe, U. Rauch, F. Bracher, S. Knapp, *Chem. Biol.* **2011**, *18*, 67 – 76.
[20] D. Branton, D. W. Deamer, A. Marziali, H. Bayley, S. A. Benner, T. Butler, M. Di Ventra, S. Garaj, A. Hibbs, X. Huang, S. B. Jovanovich, P. S. Krstic, S. Lindsay, X. S. Ling, C. H. Mastrangelo, A. Meller, J. S. Oliver, Y. V. Pershin, J. M. Ramsey, R. Riehn, G. V. Soni, V. Tabard-Cossa, M. Wanunu, M. Wiggin, J. A. Schloss, *Nat. Biotechnol.* **2008**, *26*, 1146 – 1153.
[21] "Data from pocket-sized genome sequencer unveiled": E. C. Hayden, *Nature* **2014**, DOI: 10.1038/nature.2014.14724.
[22] H. Bayley, B. Cronin, A. Heron, M. A. Holden, W. L. Hwang, R. Syeda, J. Thompson, M. Wallace, *Mol. Biosyst.* **2008**, *4*, 1191 – 1208.

Received: April 6, 2015
Published online: June 8, 2015

